Results in Engineering 16 (2022) 100674

Contents lists available at ScienceDirect

Results in Engineering

journal homepage: www.sciencedirect.com/journal/results-in-engineering

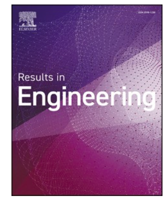

Comparative degradation analysis of accelerated-aged and field-aged crystalline silicon photovoltaic modules under Indian subtropical climatic conditions

Roopmati Meena [a,*,1], Manish Kumar [b,1], Sagarika Kumar [c,1], Rajesh Gupta [a]

[a] Department of Energy Science and Engineering, Indian Institute of Technology Bombay, Mumbai, India
[b] Department of Solar Power Systems, Institute for Energy Technology, Kjeller, Norway
[c] Dubai Electricity and Water Authority, Dubai, United Arab Emirates

ARTICLE INFO

Keywords:
Degradation analysis
Field-aged PV modules
Humidity freeze
Damp heat
Thermal cycling

ABSTRACT

The understanding of the degradation modes in end-of-life (EoL) photovoltaic (PV) modules is essential to develop realistic and effective accelerated testing methods. In this paper, types of defects and degradations (D&Ds) observed in EoL field-aged modules (FAM) have been compared with the accelerated-aged modules (AAM) for their type and underlying mechanisms. For this purpose, the FAM exposed to outdoor environmental conditions for 20 years have been taken from two cities in India. The observed D&Ds in FAM were compared with modules subjected to the temperature and humidity accelerated tests as per IEC 61215-2 standards using visual inspection, electroluminescence imaging, microscopic inspection, and current-voltage measurement. Encapsulant discoloration and delamination were the dominant modes of degradation observed in the FAM from both locations. Further, thermo-mechanical and mechanical breakages were more pronounced qualitatively under accelerated testing conditions. On the other hand, different types of chemical-induced degradations impacting both metallization and interconnects have been observed in varying degrees within damp heat and humidity freeze subjected AAM and FAM. The loss in electrical parameters namely, short circuit current and fill factor has been observed to vary in FAM and AAM subjected to different stress conditions based on the loss incurring mechanism of dominant degradation modes. The comparative analysis highlights the need for the development of effective sequential aging tests which can take into account the actual mix of external environmental conditions responsible for the various mechanism of degradation in the PV modules.

1. Introduction

Photovoltaic (PV) modules are a crucial element of a solar PV plant and their reliable operation for a guaranteed lifespan is significant for all the stakeholders involved [1]. Owing to path-breaking research and development in crystalline silicon (c-Si) PV module technology and a drastic reduction in the production cost, utility-scale PV plants have started dotting major landscapes around the globe covering key habitable climates zones [2–4]. Wherein, PV modules are subjected to different sets of environmental stresses based on the local climatic conditions, causing PV modules to suffer from various types of defects and degradations (D&Ds). The type and magnitude of D&Ds vary based on the extent of stress factors [5–10]. Thus, it is important to understand and investigate the individual and combined effect of different environmental stresses like high temperature, humidity, irradiation, high wind, etc., on the various component of a PV module. For this purpose, researchers have extensively used accelerated aging tests specified under IEC 61215-2 standard for terrestrial PV modules to investigate the operation of PV modules under various stress factors [11–13]. These test protocols apply the environmental stress factors to the PV module in an accelerated frame to unmask various degradation mechanisms in the module in a short period to assess its reliability [14].

Various studies have been carried out using different accelerated aging tests to assess module reliability under specific stress factors [15–18]. Pooja et al. [19] and Roy et al. [20] have analyzed the capacity of PV modules to withstand mechanical fatigue, thermal mismatch, and other stresses caused due to repeated changes in temperature using the

* Corresponding author.
E-mail addresses: meenaroopmati@iitb.ac.in (R. Meena), naik.manish17@gmail.com (M. Kumar), sagarika.kumar@dewa.gov.ae (S. Kumar), rajeshgupta@iitb.ac.in (R. Gupta).
[1] These authors are first authors and have contributed equally to this work.

https://doi.org/10.1016/j.rineng.2022.100674
Received 6 July 2022; Received in revised form 16 September 2022; Accepted 27 September 2022
Available online 28 September 2022
2590-1230/© 2022 The Authors. Published by Elsevier B.V. This is an open access article under the CC BY-NC-ND license (http://creativecommons.org/licenses/by-nc-nd/4.0/).

List of abbreviations and nomenclature

AAM	Accelerated-aged PV modules
A	Ampere
CCD	Charged coupled device
PC	Computer
c-Si	Crystalline silicon
I–V	Current-voltage
DH	Damp heat
D&Ds	Defects and Degradations
EL	Electroluminescence
EoL	End-of-life
FAM	Field-aged PV modules
FF	Fill factor
HF	Humidity freeze
IEC	International Electrotechnical Commission
P_{dry}	Lowest precipitation during summer
T_{cold}	The lowest temperature during winter
P_{mp}	Maximum power
V_{oc}	Open circuit voltage
PV	Photovoltaics
PID	Potential induced degradation
R_s	Series resistance
STC	Standard testing conditions
I_{sc}	Short circuit current
AgO	Silver oxide
TC	Temperature cycling
UV	Ultraviolet
UVI	Ultraviolet index
V	Volt
W	Watt

thermal cycling (TC) test and mechanical load test. They have identified wafer cracks and finger breakage at the busbar-finger interface in the post-test investigation. Similarly, Kumar et al. [21] and Kim et al. [22] have investigated moisture-ingression-induced degradation in PV modules using damp heat (DH) test in the c-Si PV modules. Wherein, the moisture ingression facilitated by high temperature conditions has resulted in corrosion of metallization at various locations within the PV modules namely, solder joint, fingers at cell edges and around cracks, and interconnect ribbon. Hamsini et al. [23] have evaluated the effect of ultraviolet (UV) radiation on the encapsulant layer of PV modules from two different manufacturers. PV modules have been subjected to different temperature conditions with exposure to UV radiation and the activation energy for encapsulant browning was calculated. It must be noted that the various accelerated aging tests defined under IEC 61215-2 standard were primarily designed to examine the PV modules for defects or faults that may occur in a short operation span under outdoor operating conditions.

In order to investigate the long-term effects of environmental stresses, various tests under IEC 61215-2 standard have been extended beyond the specified cycles to induce degradation modes in the PV modules [24,25]. A few studies have also combined multiple accelerated aging tests to closely replicate the outdoor environment conditions [16,26,27]. Owen-Bellini et al. [28] analyzed different degradation modes in the PV module by simultaneously applying multiple stress factors in two phases. Herein, the first phase was to replicate tropical climates by applying high humidity and high-temperature conditions, while the second phase was to replicate continental or desert climates by applying low humidity and high-temperature swings. Various failure modes were observed such as backsheet cracking, cell cracking, corrosion, discoloration, backsheet delamination/warping, solder-interconnect ribbon fatigue, and light-induced degradation. However, the stress factors applied in extended accelerated tests depends on the degree of extension of the test cycles [29–32]. As such, accelerated aging tests may differ from the actual extent of degradation occurring in field-operating PV modules under different climatic conditions. Therefore, there is a need to understand the difference in the type of D&Ds occurring under different outdoor environmental conditions and accelerated environmental conditions.

In this regard, a comparative analysis has been performed between field-aged modules (FAM) and accelerated-aged modules (AAM) to investigate the distinction between D&Ds occurring under outdoor and accelerated aging conditions has been performed in this paper. For this purpose, the D&Ds originating under Indian subtropical environmental conditions have been chosen to compare the effects of moisture and high temperature, which are prevalent in this region. The degradation modes observed in the PV modules under field conditions have been compared with modes that occurred in accelerated aging test conditions for the assessment of failure mechanisms. The FAM used in this study have been exposed to outdoor environmental conditions for around 20 years in two cities of India, namely, Delhi and Mumbai. Moreover, accelerated aging tests have been performed on unaged PV modules as per IEC 61215-2 standards to simulate the effects of humidity and temperature in a short period of time. These accelerated aging tests include the humidity freeze (HF) test, TC test, and DH test.

In order to investigate the PV modules exposed to the field and accelerated aging test conditions, various spatial and non-spatial techniques have been used to explore the degradation mechanism. In this paper, visual inspection, electroluminescence (EL) imaging, microscopic inspection, and current-voltage (I–V) curve measurements have been used. The outline of this paper is as follows. The detailed methodology along with the specifications of the characterization techniques and the PV modules used has been given in Section 2. Various types of D&Ds identified in FAM and AAM have been presented in Section 3. A brief discussion on D&Ds under FAM and AAM has been given in Section 4. Finally, the main conclusions of the study have been given in Section 5.

2. Methodology

In this work, a systematic approach has been used for comparative analysis of the FAM and AAM to identify the difference in the degradation modes under field aging and accelerated aging conditions considering Indian subtropical climatic conditions. The schematic of the methodology used in this work is given in Fig. 1.

The FAM have been obtained from two cities in India, viz., Delhi and Mumbai, where they were exposed to outdoor field conditions for around 20 years. Based on the most frequent operating conditions, Mumbai and Delhi have similar values of irradiance and temperature in the range of 700–750 W/m^2 and 50–55 °C, respectively [33]. Moreover, both the cities are located in high humidity region [34]. However, geographically they have different locations, Delhi lies in the Northern plains whereas Mumbai lies in Western coastal plains of India. Six FAM have been removed from the installation sites for comparative degradation analysis. On the other hand, eight unaged PV modules have been procured for accelerated aging testing and have been subjected to HF, TC, and DH test as per IEC 61215-2 standards. The initial electrical parameters of AAM before subjecting them to accelerated testing have been obtained using I–V curve measurement (flash test) for reference. The rated initial electrical parameters of the FAM and AAM are given in Table 1.

The cells used in both AAM and FAM are based on screen-printing PV technology with similar module configuration and attributes as given in Table 2.

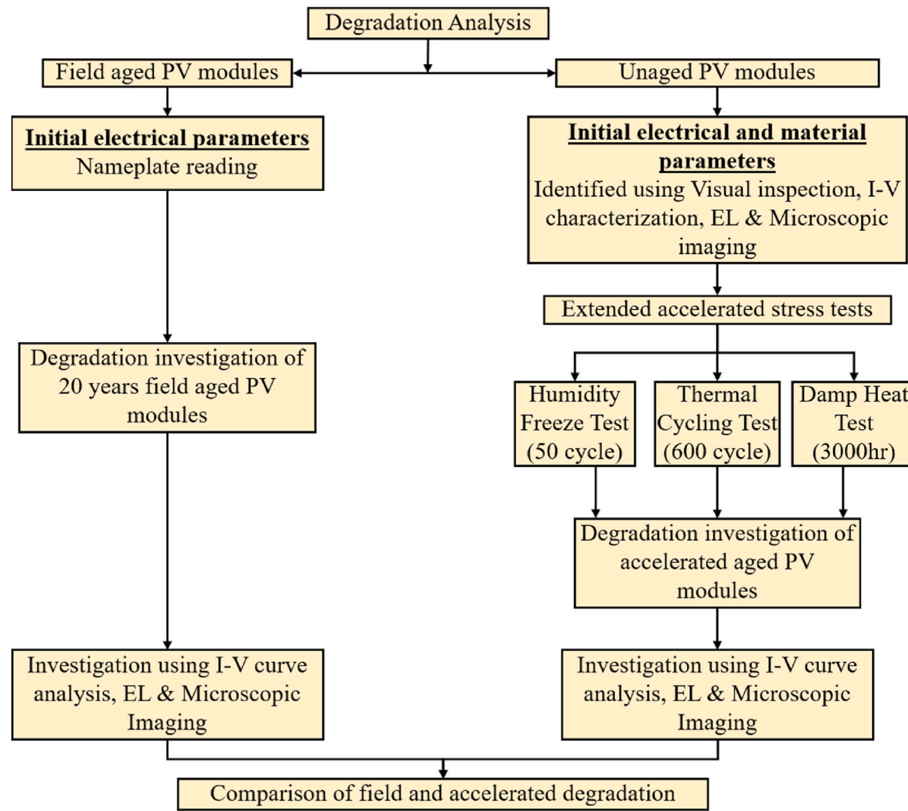

Fig. 1. Schematic of the methodology followed for the comparative analysis.

Table 1
Initial electrical parameters of PV modules used in this study.

Modules	I_{SC} (A)	V_{OC} (V)	FF (%)	P_{MP} (W)
Field-aged Module (FAM)	4	22	68	60
Accelerated-aged module (AAM)	1.7	24	75	28.36

Table 2
Characteristics of FAM and AAM used in this study.

Module Characteristics	FAM	AAM
Cell type	Full cell	Cut cell
Cell dimension	15.6 × 15.6 cm^2	15.6 × 4 cm^2
Cell technology	Multi and mono-crystalline	Multi crystalline
Number of cells in module	36	
Front metallization	Screen-printed	
Back metallization	Al-BSF	
Encapsulant	Ethylene vinyl acetate (EVA) co-polymer	
Module assembly	Glass-EVA-cell-EVA-backsheet	

2.1. Accelerated aging test

For a better understanding of degradation mechanisms and to assess the suitability of accelerated aging tests, the unaged PV modules have been aged under accelerated environment conditions. The modules were subjected to HF test, TC test, and DH test conditions. Standard test cycles according to IEC 61215-2 have been extended up to 600 cycles for TC test and 50 cycles for HF test, respectively. While DH test has been performed for 3000 h [35]. These standard test procedures have been performed in a dedicated environmental chamber (Weiss, WKS 3–1500/70/5).

2.2. Degradation investigation methods

The PV modules subjected to accelerated aging tests were pre-characterized using visual inspection, I–V curve measurement, EL imaging, and microscopic inspection for reference purposes. The prior investigation and characterization helps in identifying the various pre-existing D&Ds in the PV modules. Thereafter, the PV modules were subjected to different accelerated aging conditions to induce various degradation mechanisms. On the other hand, the FAM taken from two cities in India have been used for comparative degradation analysis with AAM. The FAM have also been characterized using above-mentioned techniques for the investigation of end-of-life (EoL) degradation mechanisms. Spatial analysis has been performed using EL imaging and microscopic inspection, while for non-spatial analysis I–V curve measurements have been performed to obtain the global effect of various D&Ds.

The D&Ds in PV modules has been characterized using EL imaging, where region having D&Ds showed a low radiation intensity that appeared as a dark spot in the EL images. The EL setup consisted of the c-Si PV module (FAM and AAM), a programmable power supply, a computer (PC), and a silicon-based charged coupled device (CCD) camera. The PV module has been excited with the help of the programmable power supply by applying forward bias at its short circuit current (I_{sc}) value. Also, to avoid noise in the measurement from stray light, the experiment has been conducted in a dark room with a constant temperature of 25 °C. The data recording time has been kept the same for all the measurements as 3 s.

Digital microscopic imaging has been used to generate magnified images of small D&Ds in PV modules, which are difficult to observe through bare eyes. A digital microscope utilizing optics and a digital camera has been used to capture images which are analyzed in an attached PC. The digital microscope magnifies the images by 400× and the results are visible on a computer monitor in real-time. During modules inspection, the digital camera has been slowly moved over the

entire area of FAM and AAM to carefully capture the D&Ds.

The I–V curve measurements of FAM and AAM has been performed to obtain an overall change in different electrical parameters for degradation analysis. For this purpose, a computer controlled module sun simulator (QuickSun-700) having xenon-single flash as light source has been used. The system has been calibrated using unaged reference module having similar cell technology, wattage, and area as the modules used this study. The computer controlled sun simulator traces the I–V curve and calculates the electrical parameters of the module while varying the load across the PV module. All the measurements have been performed at standard test conditions (STC) (AM 1.5 G, 25 °C, and 1000 W/m^2).

3. Results and discussion

In this section, the D&Ds observed in the FAM and AAM have been discussed in detail. Herein, the analysis of six 20-year-old FAM performed using visual inspection, microscopic inspection, EL imaging, and I–V curve measurement has been presented in detail. Similarly, the analysis of eight AAM subjected to HF, TC, and DH tests; and their comparative analysis with FAM has also been presented.

3.1. Field-aged PV modules (FAM)

The six FAM exposed to outdoor field conditions for 20 years at two locations namely, Mumbai and Delhi in India have been investigated. Four of the FAM have been obtained from Mumbai and are henceforth named FAM-01, FAM-02, FAM-03, and FAM-04, and two PV module obtained from Delhi have been named FAM-05, and FAM-06. The multiple D&Ds observed in the FAM-01 during the visual inspection are shown in Fig. 2 (b), 2 (c), 2 (d), and 2 (e). Three dominant defects viz. non-uniform encapsulant discoloration, delamination, and metallization corrosion on the cells of the module have been observed. Correspondingly, a dominant signature of cell cracks (Fig. 2 (e)) can also be observed in the EL image (white enclosure) given in Fig. 2 (a). Metallization corrosion can be recognized as dark regions in the EL images encircled by the red box majorly around the cell edges. Furthermore, another type of defect observed in all the cells is burnt marks on the busbars as shown in Fig. 2 (d). The burnt marks on the interconnecting ribbons of solar cells can also be traced in the EL image as dark spots at the edge of solar cells at multiple locations (encircled by a yellow box).

In addition, microscopic images of the FAM-01 have also been taken for in-depth defect analysis as shown in Fig. 3 (a) and Fig. 3 (b). The green and brown deposits have been found on the interconnect ribbons and fingers. Similar deposits are also found on the interconnect ribbon connecting to the junction box. Also, the corrosion on the fingers of the solar cells has been observed at multiple locations and impact cracks or small area cracks are also found in the cells. These defects in the FAM-01 can also be traced from its EL image, where regions having these defects are appearing as dark regions (encircled in red) in Fig. 3 (c).

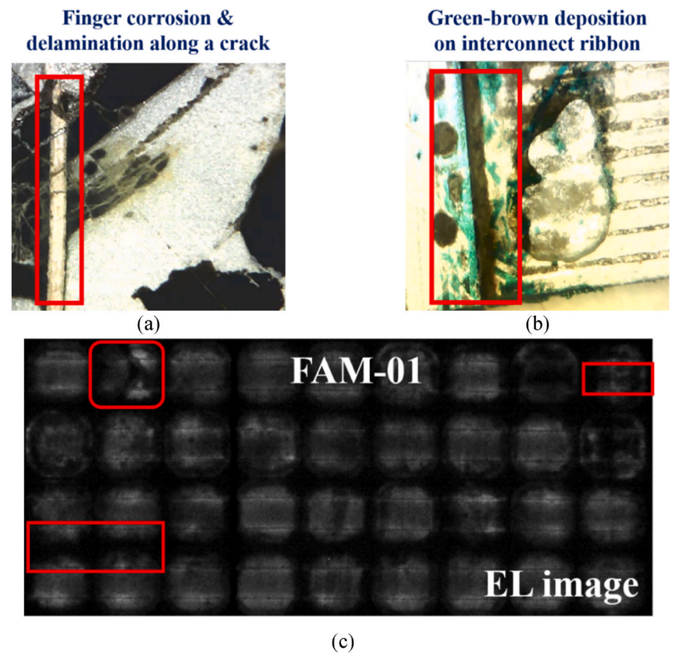

Fig. 3. Microscopic images at 400× zoom of (a) finger corrosion along a crack, (b) corrosion at interconnect ribbon, and (c) EL image of FAM-01 taken at I_{sc} of the module for a duration of 3 s.

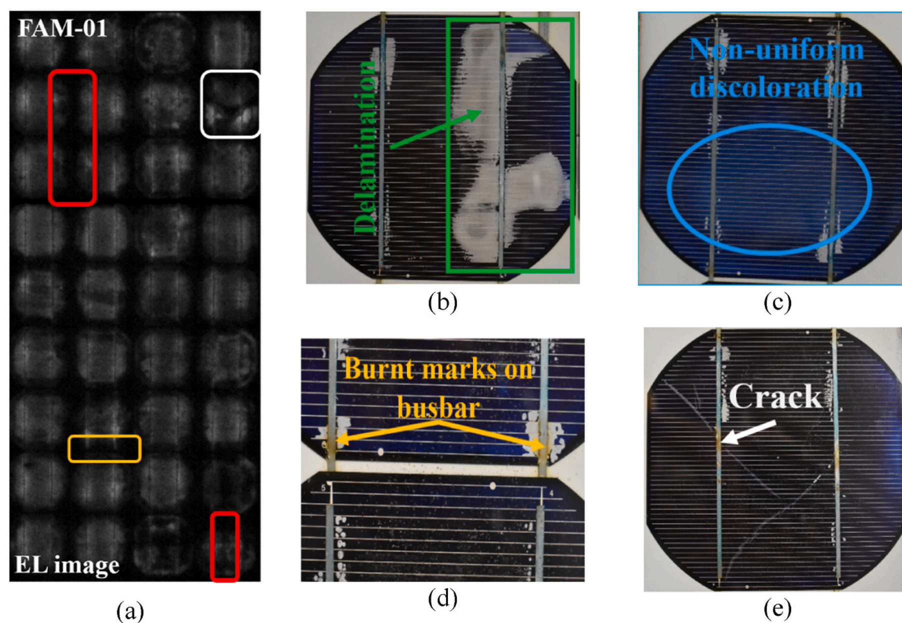

Fig. 2. (a) EL image of FAM-01 taken at I_{sc} of the module for a duration of 3 s, visual images showing (b) delamination, (c) non-uniform discoloration, (d) burnt marks on busbar, and (e) cracks in the cells of FAM-01.

The visual inspection images, microscopic images, and EL image of the FAM-02 are shown in Fig. 4. Similar to FAM-01, encapsulant delamination, corrosion in the busbar and ribbon, cracks in the cell, and encapsulant discoloration have been identified from the visual inspection of the PV module as shown in Fig. 4 (a) and Fig. 4 (b). The corresponding microscopic images have also been taken for observing minor details, as shown in Fig. 4 (c), Fig. 4 (d), Fig. 4 (e), and Fig. 4 (f). Herein, finger interruption, as well as finger corrosion at the edges of solar cell and near busbar-finger interface have been observed. Whereas, green deposits on the interconnect ribbon, fingers corrosion accompanied with delamination, and cracks, similar to FAM-01 have also been observed. Also, trapped bubbles are found in the module as shown in Fig. 4 (c), which could be evidence of moisture ingression inside the module or poor lamination process during the encapsulation process. All these degradation modes can also be traced from the EL imaging of the FAM-02 as shown in Fig. 4 (g).

Likewise, the visual inspection images, microscopic images, and EL image of the FAM-03 can be observed from Fig. 5. The encapsulant delamination, corrosion in busbar with burnt marks, encapsulant discoloration in solar cells, and diagonal cell cracks are found in the visual images of PV module as can be shown in Fig. 5 (a). Through the microscopic images shown in Fig. 5 (b), defects such as finger breakages, impact cell crack, bubbles, finger and interconnect ribbon corrosion are found. The bubbles around crack region and corrosion sites are found in the FAM indicating at the possible presence of moisture inside the modules. The EL image of the FAM-03 is shown in Fig. 5 (c). The regions corresponding to D&Ds observed in the microscopic and visual inspection have been found to have dark appearance in the EL images (encircled in EL image with corresponding colored boxes). Furthermore, the degradation analysis of the FAM-04 has also been carried out and D&Ds similar to FAM-01, FAM-02, and FAM-03 have been found in this module as well.

Further, FAM-05 and FAM-06 obtained from Delhi have also been analyzed. Visual inspection of modules showed encapsulant discoloration over the cells as a major degradation mode in FAM-05 as shown in Fig. 6 (a). It can also be observed in the corresponding EL image of FAM-05 as dark circular region (enclosed in yellow enclosure) at the centre of the solar cells as shown in Fig. 6 (b). However, the FAM-06 did not show discoloration during visual inspection. Instead, the EL image of FAM-06 showed the dark rectangular regions between the busbars and at the cell edges (enclosed in green enclosure) as shown in Fig. 6 (b). These types of pattern in EL images have been reported to occur due to finger breakages or interruption [11]. In addition, backsheet warpage also known as backsheet delamination or bubbling has been observed in both the modules.

To investigate the overall impact of the above-mentioned D&Ds on the electrical parameters in the FAM, the I–V curve analysis has been performed. The percentage degradation in electrical parameters has been calculated with respect to the nameplate parameters for the FAM as shown in Fig. 7. Herein, the loss in FF has been identified as the dominant mode of power degradation. This was followed by the loss in I_{sc} and open-circuit voltage (V_{oc}). The loss in FF can be attributed to an increase in series resistance (R_s) due to finger and interconnect corrosion, observed as green and brown deposition in the microscopic images and cracks. The loss in I_{sc} can attributed to the encapsulant discoloration, encapsulant delamination, and cracks [36].

3.2. Accelerated-aged PV module (AAM)

The accelerated aging tests including the HF test, TC test, and DH test have been carried out on unaged PV modules. For this purpose, eight unaged PV modules were primarily investigated for any pre-existing

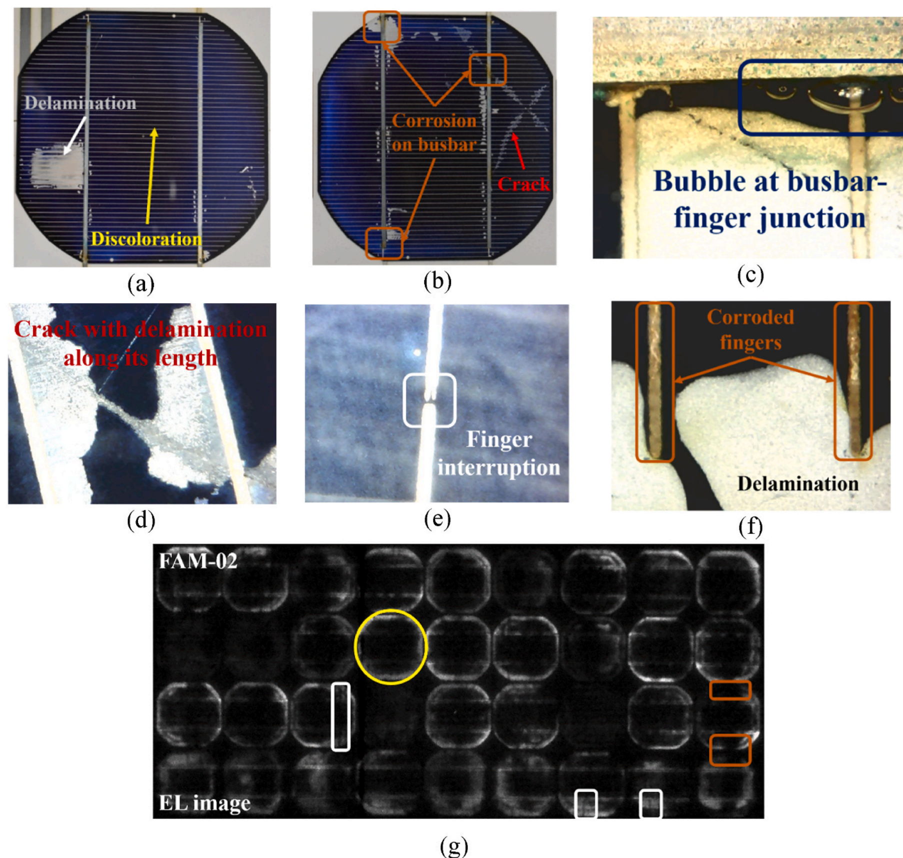

Fig. 4. Visual image showing (a) delamination & non-uniform discoloration, (b) corrosion on busbar and crack in a cell, microscopic image at 400× zoom showing (c) bubble, (d) cracks, (e) finger interruption, (f) corrosion along delaminated region, and (g) EL image of FAM-02 taken at I_{sc} of the module for a duration of 3 s.

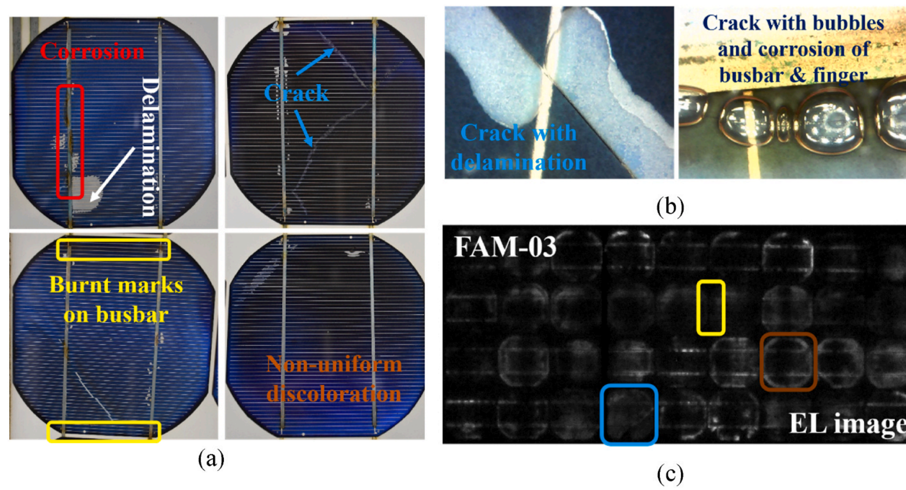

Fig. 5. (a) Visual image, (b) microscopic image at 400× zoom, and (c) EL image of FAM-03 taken at I_{sc} of the module for a duration of 3 s.

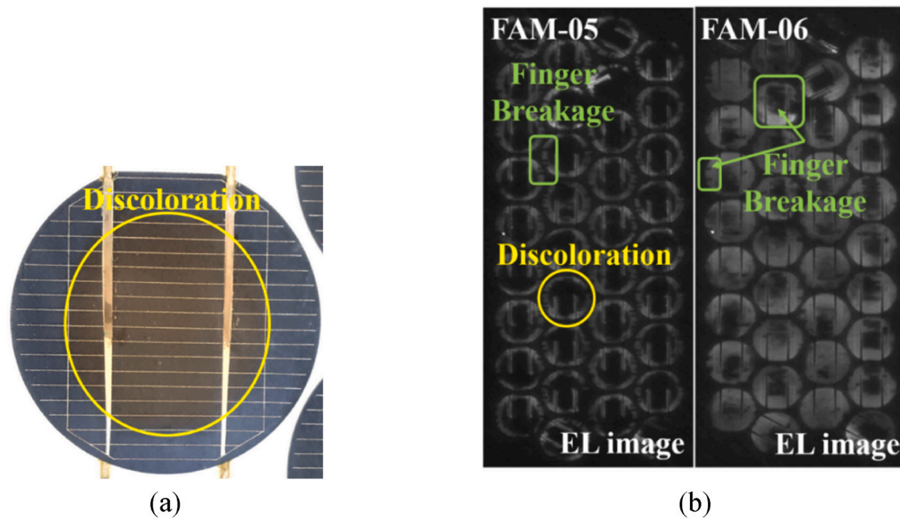

Fig. 6. (a) Visual image of discoloration in FAM-05 and (b) EL image of FAM-05 and FAM-06 taken at I_{sc} of the module for a duration of 3 s.

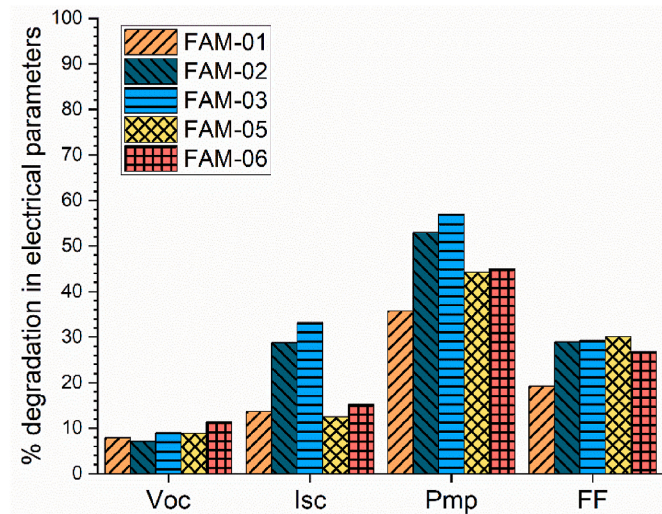

Fig. 7. Degradation in electrical parameters for 20-year-old FAM calculated from I–V curve measurement performed at STC (AM 1.5 G, 25 °C, and 1000 W/m^2).

D&Ds. Subsequently, these PV modules were subjected to different accelerated stresses in the environmental chamber. The post-test investigation has been conducted to analyze the newly formed D&Ds. These AAM have been named as AAM-01, AAM-02, AAM-03, AAM-04, AAM-05, AAM-06, AAM-07, and AAM-08 in the subsequent sections.

3.2.1. Humidity freeze (HF) test

AAM-01, AAM-02, and AAM-03 were subjected to HF testing. Herein, modules have been exposed to cyclic temperature variation with high humidity conditions. The initial and final EL images of the AAM-01 and AAM-02 have been compared. The EL images of AAM-01 as shown in Fig. 8 (a), shows multiple breakages of the fingers between interconnect ribbons, visible as dark elongated rectangular regions (enclosed in the blue box). To substantiate this fact, microscopic images of these sites have been taken and broken fingers have been detected as shown in Fig. 9 (a). Likewise, the initial and final EL image of the AAM-02 is shown in Fig. 8 (b). In the final EL image of the AAM-02, blue boxes indicate multiple finger breakages similar to AAM-01. On the other hand, the red box in the final image of AAM-01 and AAM-02 indicates the complete separation of the cell from the busbars at the edges of the cell. These can be attributed to the cyclic variation of the temperature in the HF test that induces thermo-mechanical fatigue at the busbar-finger interface which causes finger breakage [20,37].

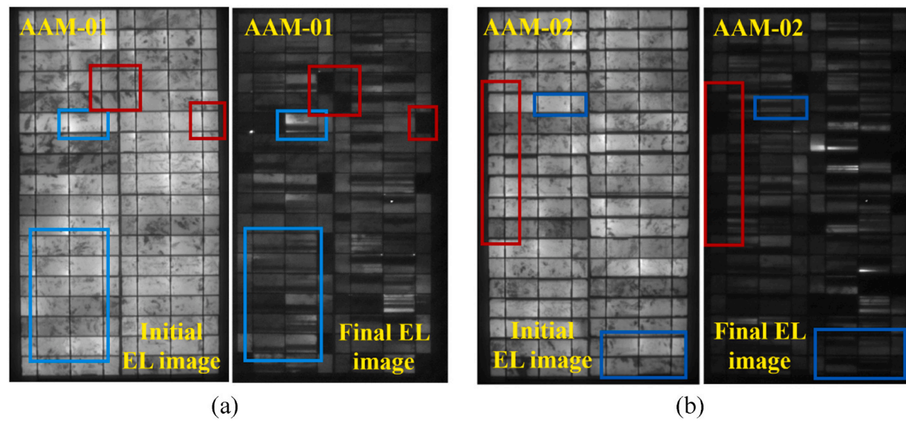

Fig. 8. The initial and final EL images of (a) AAM-01 and (b) AAM-02 subjected to 50 cycles of HF test taken at I_{sc} of the module for a duration of 3 s.

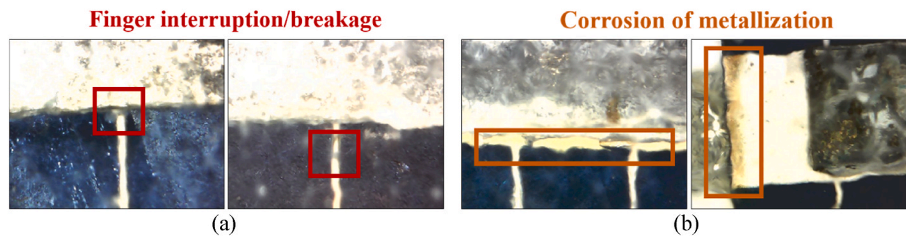

Fig. 9. Microscopic images of (a) finger interruption/breakage and (b) metallization corrosion in the AAM subjected to HF test at 400× zoom.

In addition to the multiple finger breakages as seen in the AAM-01 and AAM-02, the module named AAM-03 also showed propagation of existing cracks. The initial and final EL images of the AAM-03 are shown in Fig. 10. The brown box in the initial EL image shows the presence of crack that propagated into the severe crack in the final EL image causing the detachment of the active cell area from the busbar. The increase in the dark region around pre-existing crack regions in the final EL images indicate at the possibility of moisture ingression through cracked region. Additionally, dark patches were found around the busbars as shown in the green box of the final EL image of the AAM-03; however, there was no prior crack at this site. This indicates the presence of corrosion of metallization due to moisture ingression as observed through microscopic inspection shown in Fig. 9 (b). It must be noted that non-homogeneous dark patches are present in the final EL images at pre-existing defects sites which shows the non-homogeneous propagation of D&Ds.

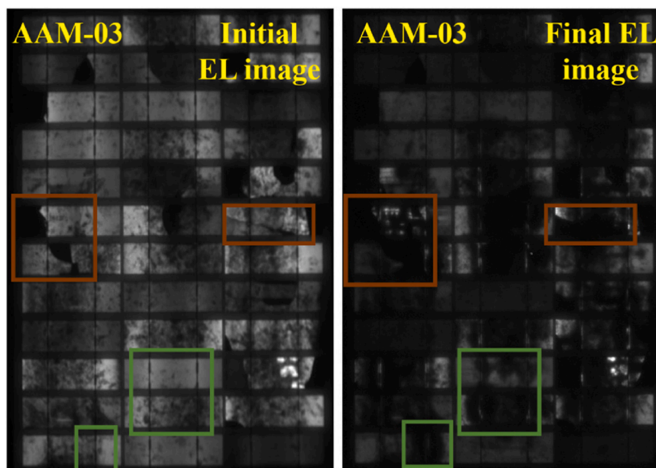

Fig. 10. Initial and final EL images of the AAM-03 subjected to 50 cycle of HF test taken at I_{sc} of the module for a duration of 3 s.

Comparative analysis of AAM subjected to HF test with FAM has also been performed. It can be observed that D&Ds found in HF test namely, finger breakages, propagation of cracks, and moisture ingression around busbar and pre-existing cracks are similar to that observed in majority of FAM. It can be attributed to the presence of cyclic temperature variation with high humidity conditions in HF test, which also co-exist under outdoor environmental conditions in Indian subtropical climatic conditions. The finger breakage has been the prevalent degradation mode under HF test. However, junction box failure and burnt marks found in the FAM, which primarily result due to long-terms exposure to harsh environmental conditions were not found in HF test subjected AAM.

Correspondingly, to investigate the electrical impact of the observed D&Ds, I–V curve analysis has been performed. The I–V curves and change in electrical parameters of AAM subjected to HF test is shown in Fig. 11 (a) and Fig. 11 (b), respectively. Herein, loss in I_{sc} was observed as the dominant mode of power degradation. Whereas, loss in FF has been low in comparison, which is contrary to the perception that finger breakages only lead to an increase in R_s, causing a loss in FF. In the HF test, the presence of high moisture content has led to corrosion of metallization causing hindrance in the current collection and additional loss in I_{sc} [38]. Moreover, the finger breakages observed under this test were multiple and in the cluster, leading to large electrically disconnected regions causing a loss in the active area of the cell for current production, thus, causing a loss in I_{sc}.

3.2.2. *Thermal cycling (TC) test*

The modules named AAM-04, AAM-05, and AAM-06 were subjected to TC test. The initial and final EL images of the AAM-04 and AAM-05 are compared as shown in Fig. 12. The multiple finger breakages have been found in the final EL image of the AAM-04 as shown in the blue box of Fig. 12 (a). A similar defect is also found in the final EL image of the AAM-05 as shown in Fig. 12 (b). In addition, at some locations all fingers between the interconnect ribbons have also been found to be broken in both AAM-04 and AAM-05, indicated as red-colored boxes in the final EL images. To validate these defects, microscopic images of these sites have

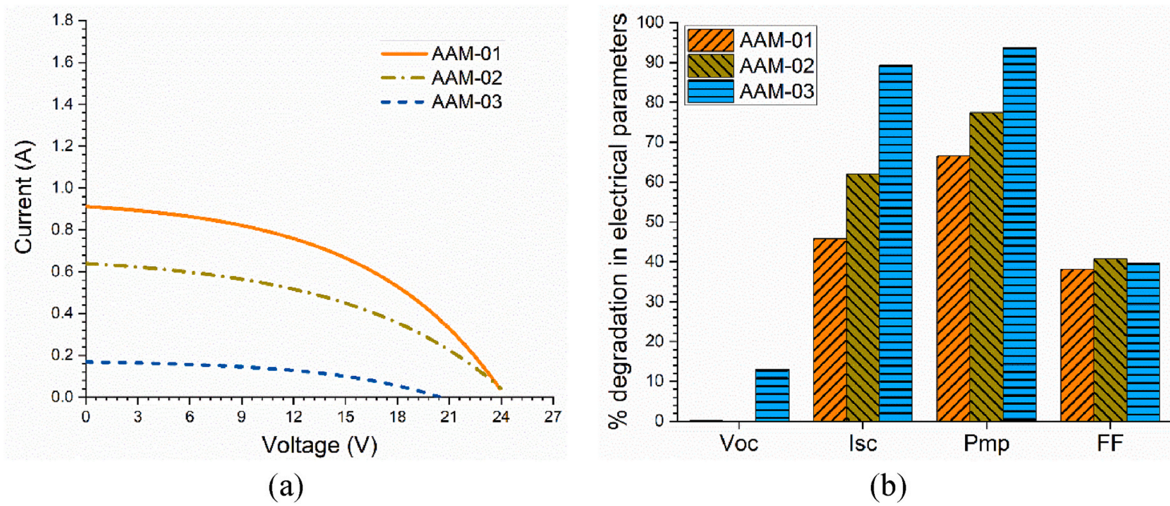

Fig. 11. (a) Current-voltage plot at standard test conditions (AM 1.5 G, 25 °C, and 1000 W/m^2) and (b) degradation in electrical parameters of AAM subjected to 50 cycle of HF test.

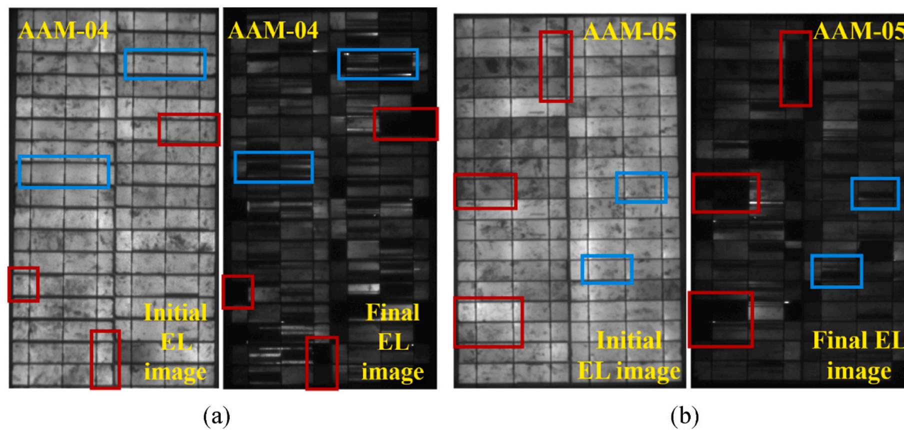

Fig. 12. The initial and final EL images of (a) AAM-04 and (b) AAM-05 subjected to 200 cycle of TC test taken at I_{sc} of the modules for a duration of 3 s.

also been taken and broken fingers have been detected.

The initial and final images of the AAM-06 are shown in Fig. 13 (a). It can be seen from the brown boxes that the area of sharp dark regions characteristic to the presence of cracks and cracks in the initial EL image has increased in the size in the final EL image indicating at the propagation of pre-existing cracks. The microscopic image of cell crack is shown in Fig. 13 (b). The red and blue boxes in EL images indicate fingers breakage at the busbar-finger interface which is similar to the degradation observed in HF test. However, in comparison to HF test, it should be noted that non-homogenous dark regions are not present in the vicinity of pre-existing cracks. Non-homogenous region in HF corresponded to humidity related degradation. Their absence in TC could

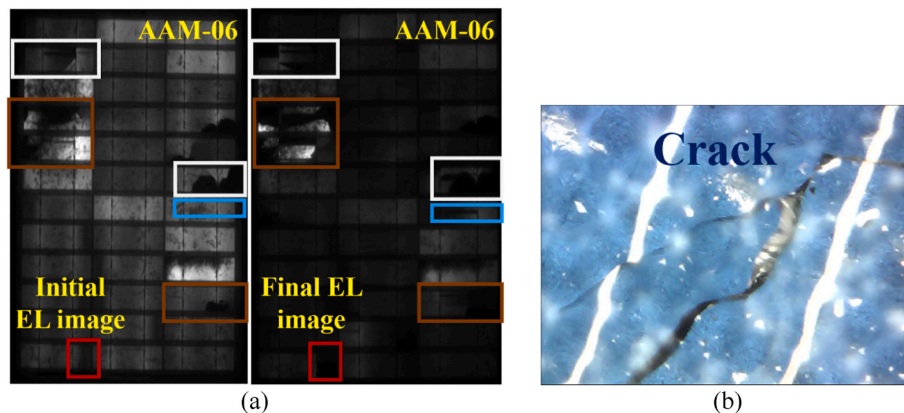

Fig. 13. (a) Initial and final EL images taken at I_{sc} of the module for a duration of 3 s and (b) microscopic image of crack at 400× zoom of the AAM-06 subjected to 200 cycles of TC test.

be due to dry conditions under TC test. However, characteristic patterns similar to finger breakages are visible around pre-existing cracks (enclosed in white box) in final EL image.

Comparative analysis with FAM shows that propagation of pre-existing cracks and finger breakages are the common degradation mode found in AAM subjected to TC test conditions and FAM. The D&Ds observed under TC are mainly due to the presence of cyclic temperature variation i.e. thermo-mechanical stress induced. However, it must be noted that the finger breakages in FAM were mostly located at the cell edges (Fig. 6 (c)). On the contrary, finger breakages in AAM appear to have originated near busbar-finger interfaces. In addition, the magnitude of finger breakages has also been more in TC subjected AAM compared to FAM. The electrical impact of the observed D&Ds has been investigated using I–V curve analysis. The I–V curve and percentage degradation in electrical parameters of AAM subjected to the TC test is given in Fig. 14 (a) and Fig. 14 (b), respectively. Herein the loss in FF has been observed as the dominant mode of power degradation. It can be attributed to the breakage of fingers, cracks, and their propagation. Further, these degradation modes also lead to a loss in I_{sc}, by hindering the collection of the current to external circuit.

3.2.3. Damp heat (DH) test

Like the HF and TC test, two unaged PV modules named AAM-07 and AAM-08 have been subjected to the DH test. The initial and final EL images of the AAM-07 and AAM-08 are shown in Fig. 15 (a) and 15 (b), respectively. The non-homogenous dark patches are found around the busbars as shown in the yellow boxes of the final EL images of the AAM-07 and AAM-08. However, the visual inspection did not reveal the presence of metallization corrosion. This type of patch around busbars without visible signature under moisture conditions can be attributed to the migration of tin from the solder material which can lead to metallization corrosion and increased R_s [39–41]. The DH test consists of high temperature and humid conditions that promote moisture ingression into the vicinity of the interconnect ribbon. In addition, some finger breakages have also been found between the interconnect ribbons and these can be seen from the red boxes in the final EL image of the AAM-08.

The propagation of pre-existing cracks has not been detected in the modules, and an example of this is shown in the EL image of AAM-08 (white box). This may be due to the absence of cyclic temperature variation in the DH test. In addition, backsheet warpages or backsheet delamination were observed in the DH test subjected AAM. The comparative analysis of D&Ds observed in DH subjected AAM with FAM shows moisture-ingression induced degradation as common degradation mode. Wherein, corrosion in interconnect ribbon and tin-migration has been found in the AAM subjected to DH test. In addition, the warpages in the backsheet near the busbar region found in DH test were also found in FAM. However, neither pre-existing crack sites have propagated, nor the dark regions around them has expanded in the DH test. It can be attributed to the absence of cyclic thermo-mechanical stress in DH test, which leads to a propagation of cracks and provides path for moisture ingression. Moreover, junction box failure and interconnect burnt marks have also not been found under DH test conditions.

The electrical impact of the D&Ds observed in the DH test has been investigated using I–V curve analysis. The plot showing, I–V curves and percentage degradation in the electrical parameters for AAM subjected to DH test is given in Fig. 16 (a) and Fig. 16 (b), respectively. It can be observed that the loss in FF is the main factor responsible for power degradation. The high losses in FF can be attributed to the increase in R_s caused due to the interconnect corrosion and migration of tin at the busbar-finger interface. Comparatively, the loss in I_{sc} is low, primarily due to the localized effect of tin migration-related degradation over the module.

4. Degradation in PV module under Indian subtropical climatic conditions

In this section, various D&Ds observed under different accelerated aging test conditions and their impact on electrical parameters have been compared with FAM under Indian subtropical climatic conditions. It has been observed that loss in FF and I_{sc} are the dominant modes of electrical power loss in both FAM and AAM. However, these two can be divided into the common mode of degradation and prominent power-degrading parameter. In the outdoor fielded modules, the FF losses showed similar variation amongst the different modules, indicating it as a more common mode of degradation. Such losses can be induced due to corrosion or breakage of metallization and cracks, which has been observed in the FAM. However, discoloration and delamination have led to a higher power degradation primarily due to loss in I_{sc}. On the other hand, I_{sc} losses showed lower variation under the TC test followed by a high severity of FF losses which can be attributed to the large number of finger breakages. Whereas, the I_{sc} losses were a common mode of degradation where the majority of finger breakages have led to complete disconnection of cell regions as in the case of PV modules subjected to HF test.

In the case of DH test subjected modules, high FF losses have been observed owing to inhomogeneous corrosion within the modules. Similarly, under the HF test low variation in FF leads to an important

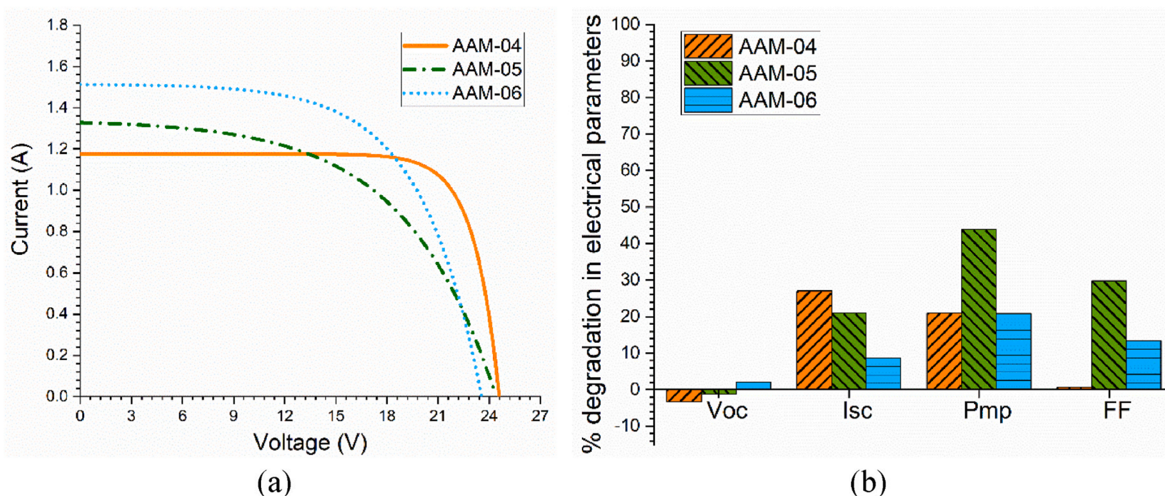

Fig. 14. (a) Current-voltage plot at standard test conditions (AM 1.5 G, 25 °C, and 1000 W/m^2) and (b) degradation in electrical parameters of AAM subjected to 200 cycles of TC test.

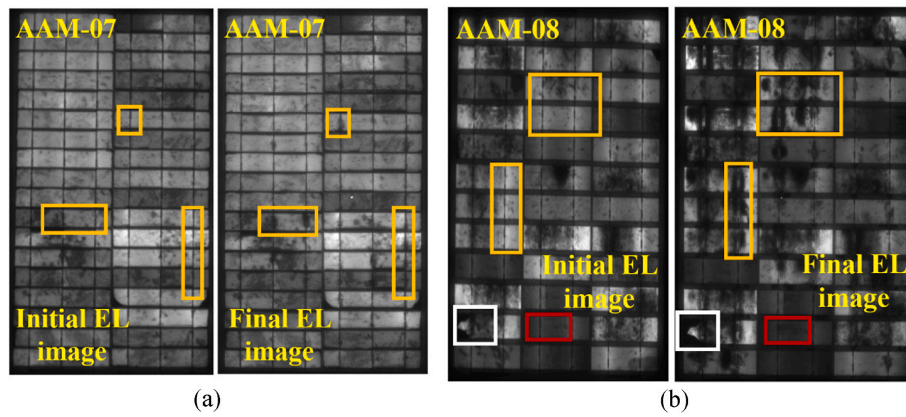

Fig. 15. The initial and final EL images of (a) AAM-07 and (b) AAM-08 taken at I_{sc} of the module for a duration of 3 s of the AAM subjected to 3000 h of DH test.

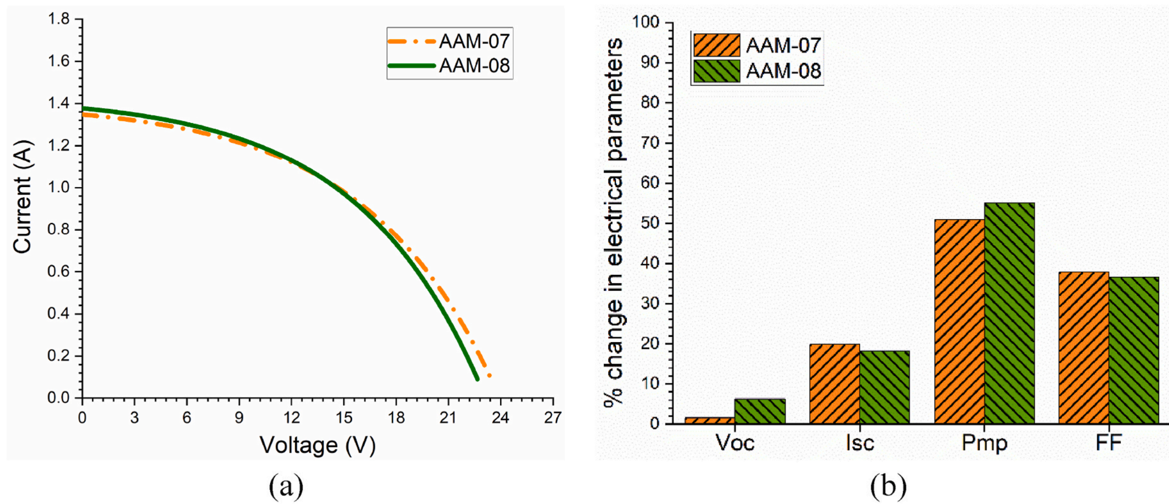

Fig. 16. (a) Current-voltage plot at standard test conditions (AM 1.5 G, 25 °C, and 1000 W/m^2) and (b) degradation in the electrical parameters of AAM subjected to 3000 h of DH test.

conclusion that both the FF and I_{sc} losses are playing an important role in degradation. Based on the analysis, it can be observed that the HF test has shown to be closest to the outdoor aged modules. It could be due to the presence of both high moisture conditions and cyclic temperature variation in the test sequence that the HF test is best able to replicate real outdoor conditions. The thermo-mechanical condition in HF test can be further used for investigation of encapsulant delamination. However, the absence of delamination in AAM could be due to difference in the size, which can yield different challenges in lamination uniformity that influences delamination susceptibility. Table 3 shows the dominant D&Ds observed in the examined modules which were subjected to different types of aging i.e., field-aged and accelerated-aged.

However, the comparative analysis shows that extent of degradation induced by the existing accelerated aging tests varies significantly in comparison to the degradation modes observed under outdoor conditions. For instance, the number of finger breakages in the AAM subjected to TC and HF test has been significantly high. While the effect of moisture ingression induced degradation has been prominent in FAM. Further, AAM did not show the presence of discoloration as the accelerated test sequences do not include UV radiation, which is primarily responsible for encapsulant discoloration in the field. Under outdoor environment conditions, the combined effect of multiple stress factors acting simultaneously on PV modules results in different degradation mechanism. Thus, there is a need to make geography-specific inclusive accelerated aging tests to replicate the actual outdoor stress conditions

Table 3
Defects and degradations under Indian climatic conditions and accelerated aging conditions.

Defects and Degradations		Field-aged modules (FAM)	Accelerated-aged modules (AAM)		
			HF	TC	DH
Encapsulant Discoloration		✓	x	x	x
Encapsulant delamination (Grey appearing)		✓	x	x	x
Finger breakage		✓	✓	✓	x
Trapped bubbles		✓	x	x	x
Finger corrosion	AgO	✓	✓	x	✓
	Inhomogeneous	✓	✓	x	✓
Interconnect corrosion		✓	✓	x	✓
Cell cracks (initiation & propagation)		✓	✓	✓	x
Burnt marks		✓	x	x	x
Junction box degradation		✓	x	x	x
Backsheet warpage or delamination		✓	x	x	✓

and understand the mechanism of degradation modes in the PV module.

The comparison of the results of this study with similar studies in the literature shows that the types of D&Ds in the PV modules are similar throughout the advancement in module design and technologies when PV modules are subjected to a given set of stress conditions.

Discoloration and delamination of encapsulant have become more prevalent under UV and high temperature conditions [42]. While cracks, corrosion of busbar and fingers, etc. found under TC, HF, and DH tests are present in the PV modules operating under outdoor conditions [43, 44]. It suggests that with the advancement in the types of cell and module technologies, the role of components and materials have become more crucial for the reliability and durability of PV module [16,45]. In addition, the extent of D&Ds found in the AAM is different than that found in FAM. The understanding of the operating mechanism of D&Ds is thus important to mitigate them at the design level. It again emphasizes the need for a combined accelerated test to replicate an actual mix of external environmental conditions to test the reliability of the new technology PV module.

5. Conclusion

In this study, a comparative analysis has been performed between types of degradation modes observed in the accelerated-aged module (AAM) and end-of-life field-aged modules (FAM) subjected to subtropical climatic conditions in India for 20 years. The AAM have been subjected to humidity freeze (HF), temperature cycling (TC), and damp heat (DH) test conditions. The common defects and degradations (D&Ds) observed in both FAM and AAM are finger breakages, metallization corrosion, cracks, corrosion of metallization around crack, and backsheet warpage or delamination. However, some of the degradation modes were specific to FAM namely, junction box degradation and delamination along the busbar. The observed D&Ds differed in terms of location of occurrence amongst FAM and AAM. In AAM, finger breakages have been observed to originate at the busbar-finger interface, while in FAM it has been observed at the cell edges. In addition, moisture ingression-induced chemical degradation in AAM subjected to HF and DH tests has primarily been observed around busbar and pre-existing crack regions. However, in the FAM, chemical degradation of metallization at cell edges and on interconnect ribbons connecting adjacent cells has been prominent.

The variation in the type, location, and magnitude of D&Ds in AAM and FAM suggests differences in their operating mechanism under field operating and accelerated aging test conditions. The impact of the difference in the operating mechanism of D&Ds in AAM and FAM has also been observed on the electrical parameters, primarily in the short circuit current (I_{sc}) and fill factor (FF) of the module. However, the extent of loss in the aforementioned parameters varied based on the dominant degradation under different stress conditions. For FAM and AAM subjected to the DH and TC test, the loss in FF was maximum, while for AAM subjected to HF test, the maximum loss was observed in I_{sc}. Based on the types of D&Ds, AAM subjected to HF test were found to be akin to FAM. However, the test conditions of individual accelerated aging tests do not replicate the actual mix of outdoor conditions. Thus, there is a need for a sequential aging test, which can more closely imitate outdoor environmental conditions. It would assist in understanding the types and underlying operating mechanisms of D&Ds originating in a specific set of outdoor conditions. For this purpose, the regional climate-specific accelerated aging test must be developed.

Credit author statement

Roopmati Meena: Conceptualization, Methodology, Investigation, Validation, Formal analysis, Data Curation, Writing- original draft, Visualisation. Manish Kumar: Conceptualization, Methodology, Investigation, Formal analysis, Writing- original draft, Visualisation. Sagarika Kumar: Investigation, Formal Analysis, Writing-review & editing. Rajesh Gupta: Conceptualization, Supervision, Resources, Project administration, Writing-review & editing.

Declaration of competing interest

The authors declare that they have no known competing financial interests or personal relationships that could have appeared to influence the work reported in this paper.

Acknowledgment

The authors would like to thank Dr. O. S. Sastry, National Institute of Solar Energy (NISE), Delhi for providing field-aged PV modules subjected to climatic conditions of Delhi to perform degradation analysis of PV modules under Indian climatic conditions.

References

[1] A.M. Al-Falahat, J.A. Qadourah, S.S. Alrwashdeh, R. khater, Z. Qatlama, E. Alddibs, M. Noor, Energy performance and economics assessments of a photovoltaic-heat pump system, Results Eng 13 (2022), 100324, https://doi.org/10.1016/j.rineng.2021.100324.
[2] U.K. Elinwa, J.E. Ogbeba, O.P. Agboola, Cleaner energy in Nigeria residential housing, Results Eng 9 (2021), 100103, https://doi.org/10.1016/j.rineng.2020.100103.
[3] S. Susan, D. Wardhani, Building integrated photovoltaic as GREENSHIP'S on site renewable energy tool, Results Eng 7 (2020), 100153, https://doi.org/10.1016/j.rineng.2020.100153.
[4] M. Gaetan, O. Sinead, R. Manoel, Global Market Outlook, 2018, https://doi.org/10.1787/key_energ_stat-2014-en.
[5] S.S. Chandel, M. Nagaraju Naik, V. Sharma, R. Chandel, Degradation analysis of 28 year field exposed mono-c-Si photovoltaic modules of a direct coupled solar water pumping system in western Himalayan region of India, Renew. Energy 78 (2015) 193–202, https://doi.org/10.1016/j.renene.2015.01.015.
[6] J.M. Kuitche, R. Pan, G. Tamizhmani, Investigation of dominant failure mode(s) for field-aged crystalline silicon PV modules under desert climatic conditions, IEEE J. Photovoltaics 4 (2014) 814–826, https://doi.org/10.1109/JPHOTOV.2014.2308720.
[7] B. Bora, O.S. Sastry, R. Kumar, R. Dubey, S. Chattopadhyay, J. Vasi, S. Mondal, B. Prasad, Failure mode analysis of PV modules in different climatic conditions, IEEE J. Photovoltaics 11 (2021) 453–460, https://doi.org/10.1109/JPHOTOV.2020.3043847.
[8] C. Borri, M. Gagliardi, M. Paggi, Fatigue crack growth in Silicon solar cells and hysteretic behaviour of busbars, Sol. Energy Mater. Sol. Cells 181 (2018) 21–29, https://doi.org/10.1016/j.solmat.2018.02.016.
[9] R. Meena, S. Kumar, R. Gupta, Comparative investigation and analysis of delaminated and discolored encapsulant degradation in crystalline silicon photovoltaic modules, Sol. Energy 203 (2020) 114–122, https://doi.org/10.1016/j.solener.2020.04.041.
[10] H. Mohammed Niyaz, R. Meena, R. Gupta, Impact of cracks on crystalline silicon photovoltaic modules temperature distribution, Sol. Energy 225 (2021) 148–161, https://doi.org/10.1016/j.solener.2021.07.038.
[11] S. Kumar, R. Gupta, Investigation and analysis of thermo-mechanical degradation of fingers in a photovoltaic module under thermal cyclic stress conditions, Sol. Energy 174 (2018) 1044–1052, https://doi.org/10.1016/j.solener.2018.10.009.
[12] C. Buerhop, S. Wirsching, A. Bemm, T. Pickel, P. Hohmann, M. Nieß, C. Vodermayer, A. Huber, B. Glück, J. Mergheim, C. Camus, J. Hauch, C.J. Brabec, Evolution of cell cracks in PV-modules under field and laboratory conditions, Prog. Photovoltaics Res. Appl. 26 (2018) 261–272, https://doi.org/10.1002/pip.2975.
[13] O.O. Ogbomo, E.H. Amalu, N.N. Ekere, P.O. Olagbegi, Effect of operating temperature on degradation of solder joints in crystalline silicon photovoltaic modules for improved reliability in hot climates, Sol. Energy 170 (2018) 682–693, https://doi.org/10.1016/j.solener.2018.06.007.
[14] L.N. Dumas, A. Shumka, Photovoltaic module reliability improvement through application testing and failure analysis, IEEE Trans. Reliab. R- 31 (1982) 228–234, https://doi.org/10.1109/TR.1982.5221325.
[15] J. Kuitche, S. Tatapudi, G. TamizhMani, A novel climate-specific field accelerated testing of PV modules, in: New Concepts Sol. Therm. Radiat. Convers, . Reliab., 2018, pp. 1–10, https://doi.org/10.1117/12.2326699.
[16] T.J. Trout, W. Gambogi, T. Felder, K.R. Choudhury, L. Garreau-Iles, Y. Heta, K. Stika, PV Module Durability -connecting field results, accelerated testing, and materials, in: Proc, IEEE PVSC, IEEE, 2018, pp. 2312–2317, https://doi.org/10.1109/pvsc.2017.8366321.
[17] S. Kajari-Schröder, I. Kunze, U. Eitner, M. Köntges, Spatial and orientational distribution of cracks in crystalline photovoltaic modules generated by mechanical load tests, Sol. Energy Mater. Sol. Cells 95 (2011) 3054–3059, https://doi.org/10.1016/j.solmat.2011.06.032.
[18] W. Gambogi, Y. Heta, K. Hashimoto, J. Kopchick, T. Felder, S. MacMaster, A. Bradley, B. Hamzavytehrany, L. Garreau-Iles, T. Aoki, K. Stika, T.J. Trout, T. Sample, A comparison of key PV backsheet and module performance from fielded module exposures and accelerated tests, IEEE J. Photovoltaics 4 (2014) 935–941, https://doi.org/10.1109/JPHOTOV.2014.2305472.
[19] P. Chaturvedi, B. Hoex, T.M. Walsh, Broken metal fingers in silicon wafer solar cells and PV modules, Sol. Energy Mater. Sol. Cells 108 (2013) 78–81, https://doi.org/10.1016/j.solmat.2012.09.013.

[20] S. Roy, S. Kumar, R. Gupta, Investigation and analysis of finger breakages in commercial crystalline silicon photovoltaic modules under standard thermal cycling test, Eng. Fail. Anal. 101 (2019) 309–319, https://doi.org/10.1016/j.engfailanal.2019.03.031.
[21] S. Kumar, R. Meena, R. Gupta, Imaging and micro-structural characterization of moisture induced degradation in crystalline silicon photovoltaic modules, Sol. Energy 194 (2019) 903–912, https://doi.org/10.1016/j.solener.2019.11.037.
[22] T.H. Kim, N.C. Park, D.H. Kim, The effect of moisture on the degradation mechanism of multi-crystalline silicon photovoltaic module, Microelectron. Reliab. 53 (2013) 1823–1827, https://doi.org/10.1016/j.microrel.2013.07.047.
[23] H. Gopalakrishna, A. Sinha, K. Dolia, D. Jordan, G. Tamizhmani, Nondestructive characterization and accelerated UV testing of browned field-aged PV modules, IEEE J. Photovoltaics 9 (2019) 1733–1740, https://doi.org/10.1109/JPHOTOV.2019.2927920.
[24] W. Herrmann, N. Bogdanski, Outdoor weathering of PV modules - effects of various climates and comparison with accelerated laboratory testing, Conf. Rec. IEEE Photovolt. Spec. Conf. (2011), https://doi.org/10.1109/PVSC.2011.6186415.
[25] N. Kim, H. Kang, K.J. Hwang, C. Han, W.S. Hong, D. Kim, E. Lyu, H. Kim, Study on the degradation of different types of backsheets used in PV module under accelerated conditions, Sol. Energy Mater. Sol. Cells 120 (2014) 543–548, https://doi.org/10.1016/j.solmat.2013.09.036.
[26] I. Kaaya, M. Koehl, A.P. Mehilli, S. De Cardona Mariano, K.A. Weiss, Modeling outdoor service lifetime prediction of PV modules: effects of combined climatic stressors on PV module power degradation, IEEE J. Photovoltaics 9 (2019) 1105–1112, https://doi.org/10.1109/JPHOTOV.2019.2916197.
[27] J.H. Wohlgemuth, S. Kurtz, Reliability testing beyond qualification as a key component in photovoltaic's progress toward grid parity, IEEE Int. Reliab. Phys. Symp. Proc. (2011) 551–556, https://doi.org/10.1109/IRPS.2011.5784534.
[28] M. Owen-Bellini, P. Hacke, D.C. Miller, M.D. Kempe, S. Spataru, T. Tanahashi, S. Mitterhofer, M. Jankovec, M. Topič, Advancing reliability assessments of photovoltaic modules and materials using combined-accelerated stress testing, Prog. Photovoltaics Res. Appl. 29 (2021) 64–82, https://doi.org/10.1002/pip.3342.
[29] J.H. Wohlgemuth, M.D. Kempe, Equating damp heat testing with field failures of PV modules, Conf. Rec. IEEE Photovolt. Spec. Conf. (2013) 126–131, https://doi.org/10.1109/PVSC.2013.6744113.
[30] C.R. Osterwald, T.J. McMohan, History of accelerated and qualification testing of terrestrial photovoltaic modules: a literature review, Prog. Photovoltaics Res. Appl. 17 (2009) 11–33, https://doi.org/10.1002/pip.
[31] W. Herrmann, N. Bogdanski, F. Reil, M. Köhl, K.-A. Weiss, M. Assmus, M. Heck, PV module degradation caused by thermomechanical stress: real impacts of outdoor weathering versus accelerated testing in the laboratory, Reliab. Photovolt. Cells, Modul. Components, Syst. III. 7773 (2010) 77730I, https://doi.org/10.1117/12.859809.
[32] P. Hülsmann, K.-A.A. Weiss, Simulation of water ingress into PV-modules: IEC-testing versus outdoor exposure, Sol. Energy 115 (2015) 347–353, https://doi.org/10.1016/j.solener.2015.03.007.
[33] H. Mohammed, M. Kumar, R. Gupta, Mapping of most frequent operating condition of photovoltaic module across India, Sustain. Energy Technol. Assessments 47 (2021), 101369, https://doi.org/10.1016/j.seta.2021.101369.
[34] Envitrans, Indian climate, (n.d.). https://www.indianclimate.com/relative-humidity-data.php?request=5DWH4PLGSL (accessed February 22, 2022).
[35] IEC 61215-2: 2021, International Electrotechnical Commission, Terrestrial Photovoltaic (PV) Modules - Design Qualification and Type Approval - Part 2: Test Procedures, 2021.
[36] F. Li, V.S.P. Buddha, E.J. Schneller, N. Iqbal, D.J. Colvin, K.O. Davis, G. Tamizhmani, Correlation of UV fluorescence images with performance loss of field-retrieved photovoltaic modules, IEEE J. Photovoltaics 11 (2021) 926–935, https://doi.org/10.1109/JPHOTOV.2021.3075865.
[37] S. Kumar, R. Gupta, Decoupled effects of thermal cycle parameters on thermo-mechanical damage accumulation at fingers in crystalline silicon photovoltaic modules, Microelectron. Eng. 217 (2019), 111102, https://doi.org/10.1016/j.mee.2019.111102.
[38] R. Asadpour, X. Sun, M.A. Alam, Electrical signatures of corrosion and solder bond failure in c-Si solar cells and modules, IEEE J. Photovoltaics 9 (2019) 759–767, https://doi.org/10.1109/JPHOTOV.2019.2896898.
[39] R. Meena, S. Kumar, R. Gupta, Investigation and analysis of chemical degradation in metallization and interconnects using electroluminescence imaging in crystalline silicon photovoltaic modules, Conf. Rec. IEEE Photovolt. Spec. Conf. (2020) 2596–2599, https://doi.org/10.1109/PVSC45281.2020.9300539, 2020-June.
[40] N. Iqbal, D.J. Colvin, E.J. Schneller, T.S. Sakthivel, R. Ristau, B.D. Huey, B.X.J. Yu, J.N. Jaubert, A.J. Curran, M. Wang, S. Seal, R.H. French, K.O. Davis, Characterization of front contact degradation in monocrystalline and multicrystalline silicon photovoltaic modules following damp heat exposure, Sol. Energy Mater. Sol. Cells 235 (2022), 111468, https://doi.org/10.1016/j.solmat.2021.111468.
[41] Y. Ino, S. Asao, K. Shirasawa, H. Takato, Effect of Soldering on the Module Degradation along Bus Bar in DH Test and PCT for Crystalline Si PV Modules, 2018 IEEE 7th World Conf. Photovolt. Energy Conversion, WCPEC 2018 - A Jt, Conf. 45th IEEE PVSC, 28th PVSEC 34th EU PVSEC, 2018, pp. 3552–3557, https://doi.org/10.1109/PVSC.2018.8548219.
[42] N.C. Park, J.S. Jeong, B.J. Kang, D.H. Kim, The effect of encapsulant discoloration and delamination on the electrical characteristics of photovoltaic module, Microelectron. Reliab. 53 (2013) 1818–1822, https://doi.org/10.1016/j.microrel.2013.07.062.
[43] G.C. Eder, Y. Voronko, C. Hirschl, R. Ebner, G. Ujvari, W. Muhleisen, Non-destructive failure detection and visualtization of artifically and nautrally aged PV modules, Energies 11 (2018) 1–14.
[44] R. Meena, M. Kumar, R. Gupta, Investigation of dominant degradation mode in field-aged photovoltaic modules using novel differential current-voltage analysis approach, Prog. Photovoltaics Res. Appl. (2022) 1–13, https://doi.org/10.1002/pip.3580.
[45] J. Tracy, W. Gambogi, T. Felder, L. Garreau-Iles, H. Hu, T.J. Trout, R. Khatri, X. Ji, Y. Heta, K.R. Choudhury, Survey of material degradation in globally fielded PV modules, Conf. Rec. IEEE Photovolt. Spec. Conf. (2019) 874–879, https://doi.org/10.1109/PVSC40753.2019.8981140.